ELSEVIER

Thin Solid Films 322 (1998) 108–116

thin solid films

A quasi-equilibrium model for the prediction of interlayer chemistry during diamond chemical vapor deposition

Pushpa Mahalingam, David S. Dandy *

Department of Chemical Engineering, Colorado State University, Fort Collins, CO 80523-1370, USA

Received 26 March 1997; accepted 16 October 1997

Abstract

The chemistry of the intermediate layer that develops at the interface between diamond and a non-diamond substrate during diamond chemical vapor deposition is analyzed using a thermodynamic quasi-equilibrium model. Substrates of Si, Mo, W, Ti, Ta, Fe and Ni are examined, and the physical parameters such as substrate temperature, reactor pressure, and CH_4/H_2 ratio in the gas phase required for the growth of respective metal carbides/solid carbon as intermediate layers between the substrate and diamond is predicted. The intermediate layers that are considered to be formed on Si, Mo, W, Ti, Ta, Fe, and Ni are SiC, Mo_2C, WC, TiC, TaC, Fe_3C, and Ni_3C, respectively, in addition to diamond and graphite. A quasi-equilibrium treatment of heterogeneous reactions at the gas–substrate interface is used to compute the desorption rates of volatile species formed in the reaction of gaseous H_2/H with the substrate. A phase diagram is obtained for the hydrogen and metal carbides/solid carbon (graphite, diamond). Good qualitative agreement is obtained between the model predictions and existing experimental data for the chemistry of the intermediate layer formed on the substrate at various temperatures and pressures commonly employed during diamond chemical vapor deposition.

Keywords: Diamond films; Chemical vapor deposition; Quasi-equilibrium model

1. Introduction

While diamond films are now routinely being synthesized by chemical vapor deposition (CVD) [1], the underlying nucleation and early growth stages are not completely understood. A number of experimental observations of diamond nucleation reveal that, in most cases diamond does not nucleate directly on a non-diamond substrate surface, but instead on an intermediate layer which develops at the interface between diamond and non-diamond substrate during the incubation period before diamond nucleation begins [2–19]. Depending on the substrate materials, pretreatment methods, and deposition parameters, the interlayer, formed due to the chemical interactions of activated gas species with the substrate surface, may consist of metal carbides [3–5,7,8,11,15,20–22], graphite [18], amorphous [16,17], or diamond-like carbon (DLC) [6,9,13]. It is generally agreed that the intermediate layer provides nucleation sites for diamond crystallite growth, enhances diamond nucleation densities on non-diamond substrates, and provides an opportunity for controlling the morphology, orientation, and texture of diamond films during nucleation and growth [23]. The formation of interlayers is a necessary step in the spontaneous nucleation processes of diamond on non-diamond substrates, but it alone is not sufficient for diamond nucleation to occur [24]. The formation of the interlayers and the formation rate depend not only on substrate materials and pretreatment methods but also on deposition conditions.

Distinctly different intermediate layers may form on different substrates at different rates, depending on gas compositions. For example, TiC [3,20,21], TaC [3,20,21], SiC [3–5,7,8,11,15], and Mo_2C [12] interlayers have been observed on Ti, Ta, Si, and Mo substrates, respectively, while graphite is observed to form on Ni substrates [18]. Different substrate temperatures may produce different intermediate layers on the same substrate, for example, both DLC [6,9,13,25] and SiC/Mo_2C [3–5,7,8,11,15,20–22,26] have been observed on Si/Mo substrates. Low C:H ratio and/or high substrate temperature may favor the formation of carbides, while high C:H ratio and/or low substrate temperature may lead to the formation of amor-

* Corresponding author.

phous carbon or DLC, or even the direct nucleation and growth of diamond on the substrate surface [27]. Because of the critical importance of the interlayer that forms between diamond and non-diamond substrates, the chemistry of the intermediate layer that forms on Si, Mo, W, Ti, Ta, Fe and Ni substrates for various deposition parameters is examined in the present work using a thermodynamic quasi-equilibrium (QE) model. A QE treatment of the heterogeneous reactions of H and H_2 with the substrate is of great interest since such an analysis can identify not only the predominant gas species, H_x, and C_xH_y, important during diamond CVD, but can also demonstrate the effect of varying thermodynamic parameters, such as temperature, pressure, and CH_4/H_2 ratio on the growth of the solid phase, that is, the corresponding substrate carbide, graphite or diamond. Through application of the QE model to the substrate carbide, graphite, diamond, and hydrogen system, the evaporation rates of volatile species, and the deposition rates of the substrate carbides/solid carbons are calculated for different substrate temperatures and CH_4 mole fractions. Following this analysis a phase diagram is obtained for the substrate carbide, graphite, diamond and hydrogen system. Comparisons between the predictions of the model and relevant experiments are then presented.

2. Model Formulation

The QE model of Batty and Stickney [28] is applied to the substrate-carbide, graphite, diamond, and hydrogen system. The key assumption in the model is that thermochemical equilibrium conditions exist between the carbide surface and the gaseous species desorbed from it. An advantage of the QE approach over a purely kinetic approach is the minimization of the use of kinetics to the degree that the rate expressions for the overall reactions are obtained without requiring knowledge of the detailed kinetic mechanisms of the deposition processes. Kinetic theory is used solely to obtain an expression for the rate at which molecules impinge upon the solid surface or desorb from the substrate; this expression corresponds to a boundary condition between the gas and solid phases, and it allows determination of the rates in terms of thermodynamics properties. The non-thermodynamic effect is accounted for by introducing an equilibration probability (a sticking or desorption probability) into the treatment. The non-thermodynamic effect is due to only a certain fraction of the incident molecules being adsorbed on, and subsequently 'equilibrated' to the substrate surface, and the remainder simply scattered from the reaction surface without undergoing chemical change. A similar approach was taken by Sommer et al. [29] and Wang et al. [30] in an analysis of the C–H system in relation to diamond and graphite deposition/etching during diamond CVD and the results from that study were in agreement with experimental observations. Since the growth rates of metal carbides/graphite/diamond observed during diamond CVD may be very low, implying that the competing processes of deposition and etching of solid carbide/carbon may be nearly in local equilibrium, it is reasonable to employ an equilibrium analysis to predict the interlayer formation.

Kinetic theory is used in the QE model to express the rates at which vapor species are incident on, and adsorbed species are evaporated or desorbed from, the substrate surface in terms of the partial pressures of the species. The adsorption and desorption rates are given by [31]

$$I_{C_xH_y} = \frac{\eta_{C_xH_y} P_{C_xH_y}}{\sqrt{2\pi m_{C_xH_y} kT}} \ (\mathrm{cm^{-2}\ s^{-1}}) \tag{1}$$

and

$$E_{C_xH_y} = \frac{\nu_{C_xH_y} P^{eq}_{C_xH_y}}{\sqrt{2\pi m_{C_xH_y} kT}} \ (\mathrm{cm^{-2}\ s^{-1}}), \tag{2}$$

respectively, where η and ν are the non-thermodynamic sticking (equilibration) and desorption (accommodation) coefficients, $P_{C_xH_y}$ is the partial pressure of the C_xH_y species, and $P^{eq}_{C_xH_y}$ is the partial pressure of C_xH_y species in equilibrium with the substrate surface at temperature T. Also, $m_{C_xH_y}$ is the molecular mass of C_xH_y (in grams) and k is Boltzmann's constant. The units of P and T are dyn/cm^2 and K, respectively.

Under the assumption that thermochemical equilibrium exists, thermodynamics provides a means of calculating the composition, that is, equilibrium partial pressures of the mixture of gas species in contact with the surface from the equilibrium constants, K, of the generalized reactions representative of the etching of carbides,

$$xM_qC(s) + \frac{1}{2}yH_2 \Leftrightarrow xqM(s) + C_xH_y, \tag{3}$$

or

$$xM_qC(s) + yH \Leftrightarrow xqM(s) + C_xH_y, \tag{4}$$

where M denotes a metal, q is the number of metal atoms per C atom in the metal–carbide (M_qC) molecule. Note that under thermochemical equilibrium, either of Eq. (3) or Eq. (4) is sufficient to be considered as representative of the etching of carbides, since H and H_2 are related by the equation

$$\frac{1}{2}yH_2 \Leftrightarrow yH \tag{5}$$

In this work, Eq. (3) will be considered for the etching of carbides. Assuming that the gas phase may be treated as a mixture of ideal gases, the expression for the equilibrium constant for Eq. (3) is [32]

$$K_{C_xH_y} = \frac{P_{C_xH^{eq}_y}}{\left(P^{eq}_{H_2}\right)^{y/2}} P^{y/2-1} = \exp\left[-\Delta G_{C_xH_y}/RT\right], \tag{6}$$

where $\Delta G_{C_xH_y}$ is the Gibbs free energy of the reaction forming C_xH_y, R is the gas constant, and T is the substrate temperature.

Based on Eqs. (2) and (6), the evaporation rates of C_xH_y may be expressed in terms of the equilibrium constants as

$$E_{C_xH_y} = (2\pi kT)^{\frac{1}{2}(y/2-1)} \left(\frac{\nu_{C_xH_y}}{\nu_{H_2}^{y/2}}\right)\left(\frac{m_{H_2}^{y/2}}{m_{C_xH_y}}\right)^{1/2} \times K_{C_xH_y} P^{(1-y/2)} E_{H_2}^{y/2}. \quad (7)$$

Eq. (7) may be applied to the different hydrocarbon species present in the system, and it represents a set of equations involving one more unknown than the number of equations. The additional constraint required to complete the set is derived from conservation of hydrogen at the surface,

$$I_H + 2I_{H_2} + \sum_{x,y} yI_{C_xH_y} = E_H + 2E_{H_2} + \sum_{x,y} yE_{C_xH_y}, \quad (8)$$

where $\sum_{x,y}$ denote summations over all possible hydrocarbon species. Eqs. (7) and (8) may be solved to determine the evaporation and desorption rates of C_xH_y.

The question of whether deposition or etching of substrate-carbide, graphite, or diamond occurs can be answered by comparing the flux of carbon atoms reaching the substrate surface to the flux of carbon atoms leaving the surface through the production of volatile hydrocarbons. The flux of carbon atoms to the substrate surface is given by

$$I_C = \sum_{x,y} xI_{C_xH_y}, \quad (9)$$

and the total carbon flux E_C leaving the surface via the production of volatile hydrocarbons C_xH_y, is given by

$$E_C = \sum_{x,y} xE_{C_xH_y}. \quad (10)$$

Therefore, the net rate of deposition of carbide, that is, substrate-carbide, graphite, or diamond, will be given by

$$D_{M_qC} = I_C - E_C. \quad (11)$$

Thus, if $D_{M_qC} < 0$, the deposition conditions correspond to the etching of solid carbide, while for $D_{M_qC} > 0$ the deposition parameters correspond to the deposition of solid carbide.

In the present work, the following assumptions are made to formulate the model.

1. The feed gas species are assumed to be CH_4 and H_2, because these are the predominant inlet gas species in diamond CVD [1]. The species desorbed from the substrate surface are assumed to be H, H_2, CH, CH_2, CH_3, CH_4, C_2H, C_2H_2, C_2H_4, C, C_2, and C_3. These are the species that have been reported to be found in the reaction chamber in largest concentration during diamond CVD [1]. It should be noted that, in Eq. (3) or Eq. (4), metal hydrides are not considered as vapor species since they have not been detected in the reaction chamber during diamond CVD.

2. The sticking coefficients, η, of the impinging species and the desorption coefficients, ν, of the species desorbing from the substrate are assumed to be unity. This assumption is due to the fact that empirical relationships for η and ν are difficult to formulate because experimental data do not exist in the literature for the reactions of different impinging species with the various substrate materials considered. In Eqs. (7) and (8), it may be seen that the assumption of unity sticking coefficients for all the impinging species and unity desorption coefficients for all species except H_2 from the substrate increases the evaporation rates of the volatile species from the substrate, leading to a smaller window of substrate temperature and pressure for the deposition of a solid phase such as carbides or solid carbon. The assumption of unity desorption coefficient of H_2 lowers the evaporation rates of volatile species from the substrate, leading to a larger window of substrate temperature and pressure for the deposition of an intermediate carbide/solid carbon layer on the substrate. It has been shown by Batty and Stickney [28] and Batty [33] that the results obtained by assuming sticking and desorption coefficients of unity are qualitatively similar to the results obtained assuming empirical values for sticking and desorption coefficients. Therefore, the assumption of η and ν values of unity are reasonable.

The first goal of the thermodynamic analysis is the determination of temperature dependent evaporation rates for all the vapor species considered, H_x and C_xH_y, corresponding to a given total pressure P, and incoming fluxes of C and H atoms (from a CH_4/H_2 mixture). Since the Gibbs free energy of the reaction forming C_xH_y, $\Delta G_{C_xH_y}$, is known [34], the equilibrium constant $K_{C_xH_y}$ may be calculated using Eq. (6). In Eq. (7), the evaporation rates of all vapor species, $E_{C_xH_y}$ and E_H, are expressed in terms of a single variable E_{H_2}. When these rates $E_{C_xH_y}$, E_H (from Eq. (7)) and fluxes I (from Eq. (1)) are substituted into Eq. (8) for the conservation of H atoms, a polynomial equation of degree $y_{max}/2$ in E_{H_2} is obtained, where $y_{max}/2$ is the maximum value of y for any C_xH_y species considered. (In this work, $y_{max} = 4$.) The solution for E_{H_2} is obtained by iteration.

The values of $E_{C_xH_y}$ corresponding to the solution for E_{H_2} are then substituted into Eq. (11) for the carbide/carbon deposition rate D_{M_qC}, from which it can be determined whether deposition $(D_{M_qC} > 0)$ or etching $(D_{M_qC} < 0)$ of solid carbide/carbon occurs.

3. Model Predictions

The QE model is used to predict the deposition conditions under which metal carbides such as SiC, Mo_2C, TaC, TiC, Fe_3C, Ni_3C, WC, and/or solid carbon phases such as

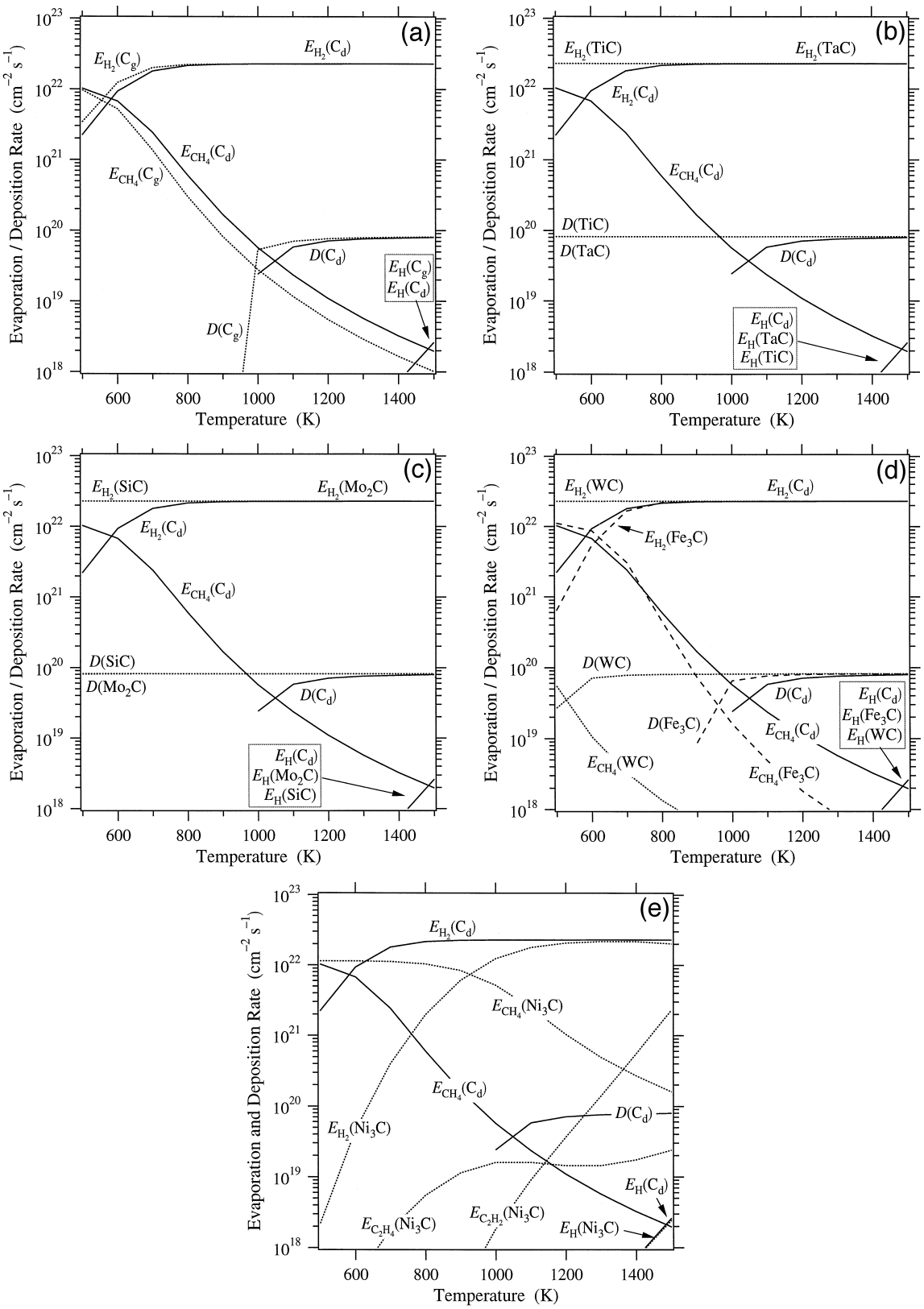

Fig. 1. The calculated predictions of the quasi-equilibrium model for the evaporative rates (E) and deposition rates (D) of hydrocarbon species, carbides, diamond (C_d), and graphite (C_g): (a) evaporation rates of various species and deposition rates of graphite and diamond; (b) evaporation rates of various species and deposition rates of TiC, TaC, and diamond; (c) evaporation rates of various species and deposition rates of SiC, Mo_2C, and diamond; (d) evaporation rates of various species and deposition rates of Fe_3C, WC, and diamond; (e) evaporation rates of various species and deposition rates of Ni_3C and diamond.

graphite or diamond may be deposited during diamond CVD. The range of substrate temperature considered in the calculations is 500–2500 K for two different reactor pressures of 36 and 760 Torr [35]. However, results are reported in this paper for the commonly used diamond CVD substrate temperature range of 500–1500 K at reactor pressures of 36 and 760 Torr. The reactor pressures of 36 and 760 Torr are chosen because both theoretical and experimental data exist in the literature for the growth of diamond at those pressures [29,36]. In Fig. 1a–e, the predictions of the QE model for the evaporation rates of species from the surface of carbides/solid carbon, are shown as functions of substrate temperature, T. The results presented in Fig. 1 are summarized in Table 1. Hydrocarbons that have been included in the model, but are not shown in Fig. 1a–e, have evaporation rates that are negligible relative to those shown, or evaporate at temperatures above 1500 K. These values of E correspond to a feed gas composition of 1% CH_4 in H_2, at a total pressure of 36 Torr. In each of the plots in Fig. 1, the deposition rate of diamond and evaporation rates of species from the diamond surface are plotted to facilitate the comparison of the deposition of carbides and evaporation rates of species from other carbide surfaces with those of diamond. As illustrated in Fig. 1a and listed in Table 1, for graphite (C_g) and diamond (C_d) the dominant reaction product is CH_4 up to approximately 600 K, and H_2 dominates from 600 K to 1500 K (the maximum substrate temperature for which results are reported). For TiC, TaC, SiC, and Mo_2C, the dominant reaction product is always H_2 throughout the substrate temperature range for which results are reported, $500 \leq T \leq 1500$ K. It may be seen in Fig. 1b and c that the evaporation rates of all the hydrocarbon species from the surface of TiC, TaC, SiC, and Mo_2C, are below 10^{18} cm^{-2} s^{-1}.

In Fig. 1d, the evaporation rates of species from the surface of WC, Fe_3C, and diamond (C_d) are plotted. Methane is the dominant reaction product for Fe_3C up to a temperature of slightly over 600 K (see Table 1), after which H_2 becomes the dominant reaction product, although CH_4 does remain the major hydrocarbon product for Fe_3C. Such a trend is also observed for both graphite (C_g) and diamond (C_d). For WC, H_2 remains the major reaction product throughout the temperature range considered in this study. Methane is the dominant hydrocarbon species for the substrate temperature range, $500 \leq T \leq 1500$ K for WC as can be seen in Table 1. In Fig. 1e, the evaporation and deposition rates for Ni_3C and diamond are plotted. Methane is the major reaction product up to 930 K, after which H_2 becomes the dominant reaction product until 1500 K (see Table 1). Methane is the dominant hydrocarbon product for the temperature range 500–1350 K, whereas C_2H_2 is the major hydrocarbon product for temperatures between 1350 and 1500 K. As illustrated in Fig. 1a–e, the partial pressures of the hydrocarbons evaporated from the solid carbides/solid carbon increase in the order $TiC < TaC < SiC < Mo_2C < Fe_3C <$ graphite $<$ diamond $< Ni_3C$. The reason for this trend in the partial pressures of evaporating species is due to the Gibbs energy of formation of the carbides and solid carbon, which varies as $Ni_3C >$ diamond $>$ graphite $> Fe_3C > WC > Mo_2C > SiC > TaC > TiC$.

Since CH_4 is present in the incoming species flux, metal carbide/solid carbon will be deposited on the surface when the incoming C flux exceeds the flux of C atoms leaving the substrate surface due to etching. The rates of deposition of metal carbide, graphite, and diamond for the inlet mixture of 1% CH_4 and 99% H_2 are shown in Fig. 1. Under these conditions, it is apparent from Fig. 1a that graphite will be deposited for substrate temperatures

Table 1
The deposition temperature range for various materials and dominant reaction species for an inlet gas mixture of 1% CH_4 in H_2 and a total reactor pressure of 36 Torr[a]

Material	Deposition temperature range (K)	Dominant species		Dominant hydrocarbons	
		Name	Temperature range (K)	Name	Temperature range (K)
Diamond	1000–1500	CH_4	500–600	CH_4	500–1500
		H_2	600–1500		
Graphite	900–1500	CH_4	500–570	CH_4	500–1500
		H_2	570–1500		
TiC	500–1500	H_2	500–1500	CH_4	500–1500
TaC	500–1500	H_2	500–1500	CH_4	500–1500
SiC	500–1500	H_2	500–1500	CH_4	500–1500
Mo_2C	500–1500	H_2	500–1500	CH_4	500–1500
Fe_3C	900–1500	CH_4	500–650	CH_4	500–1500
		H_2	650–1500		
WC	500–1500	H_2	500–1500	CH_4	500–1500
Ni_3C	–	CH_4	500–930	CH_4	500–1350
		H_2	930–1500	C_2H_2	1350–1500

[a]Computer simulations carried out for the substrate temperature range 500–1500 K.

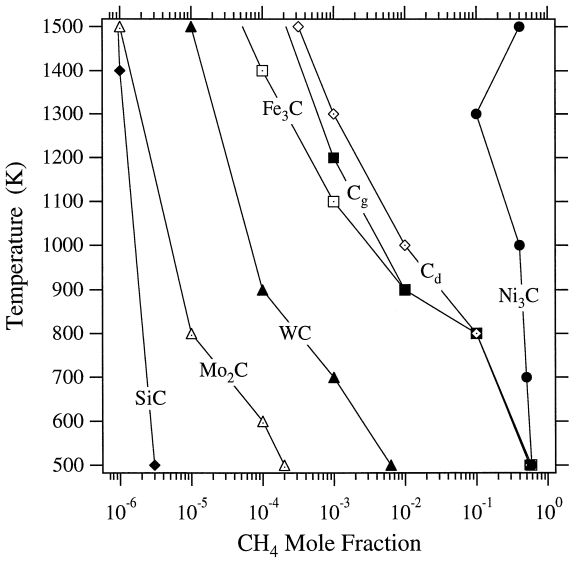

Fig. 2. The predicted phase diagram for Ni_3C, diamond (C_d), graphite (C_g), Fe_3C, WC, Mo_2C, and SiC at a total system pressure of 36 Torr.

greater than 900 K and diamond for temperatures greater than 1000 K, while SiC, Mo_2C, TiC, TaC, and WC will be deposited throughout the temperature range under consideration [cf. Fig. 1b–d] for 1% CH_4/H_2 inlet gas composition at a pressure of 36 Torr. It may be seen in Fig. 1d that Fe_3C can be deposited for substrate temperature greater than 900 K, but Ni_3C is not deposited for a 1% CH_4/H_2 inlet gas mixture and temperature between 500 K and 1500 K. It is important to point out that there is a higher temperature limit (the higher temperature limit being greater than 1500 K) beyond which diamond, graphite, and Fe_3C will not be deposited for a 1% CH_4/H_2 inlet gas composition at a pressure of 36 Torr as has been published elsewhere [35].

At a total pressure of 36 Torr the phase diagram for the metal carbide/solid carbon and hydrogen system may be obtained, as shown in Fig. 2. The boundary in the carbide/carbon–H phase diagram between etching and deposition of solid carbide/carbon will correspond to the locus of points for which $D_{M_qC} = 0$. At this pressure, it is apparent from Fig. 2 that the CH_4 mole fraction required to deposit SiC, Mo_2C, WC, Fe_3C, graphite, and diamond decreases with an increase in substrate temperature in the range $500 \leq T \leq 1500$ K. However, in the case of Ni_3C, the CH_4 mole fraction required to deposit Ni_3C decreases with an increase in substrate temperature to 1300 K after which there is an increase in the CH_4 required in the inlet gas to deposit Ni_3C; thus, Ni_3C can be deposited only for inlet CH_4 mole fractions greater than approximately 0.1. Even when inlet CH_4 concentrations are greater than the threshold value for Ni_3C stated above, Ni_3C will only be deposited in the range of temperatures between T_{low} and T_{high} for a particular CH_4 mole fraction. This is also true for the other metal carbides/solid carbon considered in this work, however, the T_{high} for the other carbides/solid carbon are greater than 1500 K, which is the maximum substrate temperature for which results are reported in this paper [35]. Etching of metal carbide/solid carbon dominates below T_{low} via the production of CH_4, as can be seen in Fig. 1a–e, and above T_{high} via the production of C_2H_2 [35]. Again, the phase boundaries in Fig. 2 correspond to $D_{M_qC} = 0$, with etching occurring to the left and deposition occurring to the right of the boundary. As illustrated in Fig. 2, the stability region of diamond lies within the stability regions of SiC, Mo_2C, WC, and graphite, that is, the model predicts that whenever diamond deposits, SiC, Mo_2C, WC and graphite also deposit. The

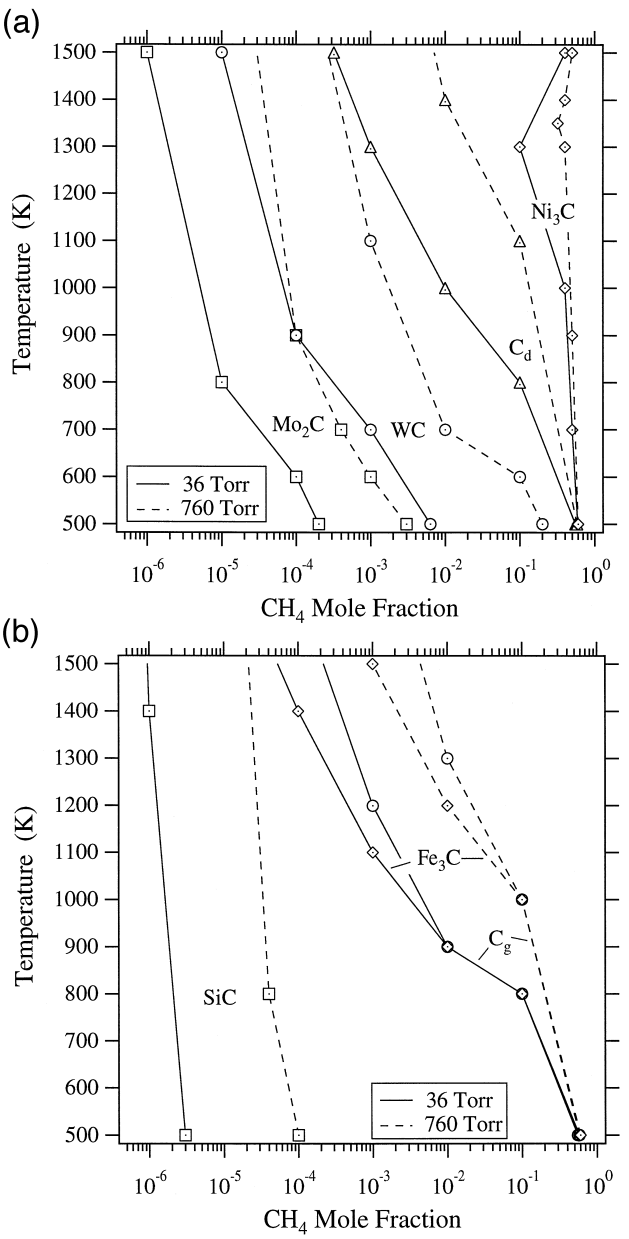

Fig. 3. The effect of total pressure on the phase diagrams of (a) Mo_2C, WC, diamond (C_d) and Ni_3C; and (b) SiC, Fe_3C, and graphite (C_g).

phase diagrams for TiC and TaC are not shown in Fig. 2 because both carbides are stable over the range of CH_4 mole fractions and temperatures considered in the plot. A thorough interpretation of the results will be discussed in Section 4.

The effect of pressure, P, on the metal carbide/solid carbon phase diagram is illustrated in Fig. 3a and b, where the phase boundary for all the different carbides and solid carbon considered are presented for two different total pressures, $P = 36$ and 760 Torr. The phase boundary for each of the carbides, diamond, and graphite shifts significantly with P. With increasing P, the boundary shifts to the right, corresponding to increased etching and a smaller stability region for all the carbides, plus diamond and graphite.

4. Discussion

In this section, the extent to which the thermodynamic analysis can aid in our understanding of the observed interlayer formation during diamond CVD will be explored for the following conditions: inlet CH_4/H_2 ratios ranging from 10^{-4} to 10^{-2}, P ranging from 30 to 760 Torr, and substrate temperatures in the range 500 to 1500 K.

The model predicts that, for Ti, Ta, Si, Mo, Fe, and W substrates, the most stable form of carbide/carbon to form immediately on the substrate surface will be TiC, TaC, SiC, Mo_2C, Fe_3C, and WC, respectively. Diamond and graphite are not likely to deposit on the substrates for the reaction conditions—substrate temperature, pressure and inlet CH_4/H_2 ratio—corresponding to the region lying to the left of the graphite phase/stability curve. This is because the graphite and diamond stability regions lie within TiC, TaC, SiC, Mo_2C, Fe_3C, and WC stability regions (see Figs. 2 and 3). If the process conditions during diamond CVD correspond to the region lying between the diamond and graphite stability curves, then the corresponding carbides as well as graphite are equally likely to form since the diamond stability curve lies within the graphite, TiC, TaC, SiC, Mo_2C, Fe_3C, and WC stability regions. If the processing parameters are such that the conditions correspond to a region lying to the right of the diamond stability curve, then the formation of diamond, graphite and TiC, TaC, SiC, Mo_2C, Fe_3C, WC are equally probable. For such conditions, the relative stability of one interlayer with respect to the other cannot be predicted by this model because to predict the stability of one material relative to others, key kinetic factors have to be introduced in the thermodynamic analysis through the inclusion of empirical values of desorption coefficients of various species from the substrate surface and realistic sticking coefficients. As discussed earlier, empirical relations for ν and η are difficult to formulate since experimental data do not exist for the desorption and adsorption of various species on the wide variety of substrates considered in this work. Hence, unity values for ν and η are assumed in this work, and as a result the predictions by the model will be qualitative in nature.

The diamond and graphite phase/stability curves at 36 Torr and 760 Torr, and the evaporation/deposition rates of various species from graphite and diamond surfaces obtained in the present work are quantitatively similar to the quasi-equilibrium results obtained by Sommer et al. [29]. The model employed by Sommer et al. showed that growth at lower temperatures or higher pressures would require higher CH_4/H_2 ratios in the inlet gas in order to remain in the diamond stability region. Wolter et al. [3] observed the formation of SiC, WC, TiC, and TaC on Si, W, Ti, and Ta substrates respectively as an interlayer prior to diamond nucleation at a substrate temperature of 973 K and a pressure of 25 Torr for a 1% CH_4/H_2 inlet gas composition. This observation is qualitatively consistent with the model predictions shown in Fig. 2, although the model also predicts the formation of graphite as an interlayer for deposition conditions used by Wolter et al. [3]. The reason graphite was not observed could be due to the enhanced etching of graphite with respect to the metal carbides, an effect not incorporated in the present quasi-equilibrium model. To explain the observed formation of selected metal carbides but not graphite in Wolter et al.'s work, several key kinetic factors would need to be included in the model; these include empirical values for the sticking and desorption coefficients of various species that would lead to the enhanced etching of graphite by hydrogen relative to the corresponding metal carbides. In an examination of WC formation, it has been reported that, at 0.2 Torr total pressure, WC is formed for a CH_4/H_2 ratio below 0.02 for a W substrate temperature of 1000°C, whereas above the 0.02 CH_4/H_2 ratio, diamond is observed to form [37]. This observation is also supported qualitatively by the model prediction. As illustrated in Figs. 2 and 3a, diamond forms at a higher CH_4 mole fraction than WC at the same temperature.

Nickel carbide is not observed to form on Ni substrates during diamond CVD. Instead, a graphite interlayer has been observed [18]. The formation of a graphite interlayer is predicted by the model (cf. Figs. 2 and 3) for Ni substrates instead of Ni_3C since the stability region of Ni_3C lies completely within that of diamond and graphite. Because of the fact that diamond's phase curve lies inside graphite's stability curve, graphite is formed first, forming directly on the Ni substrate. The experimental results available in the literature and results predicted in this study for TiC formation are now compared. Terranova et al. [38] detected graphitic clusters embedded in TiC formed on a titanium substrate prior to diamond deposition at a substrate temperature of 650 and 730°C at a total pressure of 76 Torr and inlet CH_4 concentration of 1% during diamond CVD. The temperatures at which graphite and TiC are detected are not mentioned [38]. Nevertheless, the observations by Terranova et al. [38] agree qualitatively

with the results predicted by the model in this work, illustrated in Figs. 2 and 3.

The model prediction of the shift in the etching-growth boundary of diamond to higher CH_4 mole fractions as P is increased is supported by the experiments conducted by Matsumoto et al. [36]. It was noted that diamond growth occurred between 800 and 900°C and 1% CH_4 concentration at 36 Torr, but no diamond growth was observed for the same temperature range and CH_4 concentration as P was increased to 760 Torr. This is due to the fact that the deposition conditions used at 760 Torr correspond to the etching region, so that the observed absence of diamond growth at 760 Torr is successfully explained by the QE model.

Thus, the QE model has been shown to be able to qualitatively explain the observation of the formation of interlayers such as TaC, TiC, SiC, Mo_2C, Fe_3C, WC, and graphite on Ta, Ti, Si, Mo, Fe, W, and Ni substrates for typical diamond CVD conditions. It has been postulated in the literature that intermediate layers play an important role in diamond nucleation [3,27]. For metal carbide forming substrates, it has been reported [3,27] that, for Ti, Ta, Si, Mo, and W substrates, diamond nucleation occurs on the carbide interlayer when the carbon concentration on the surface reaches its saturation value. In other words, it becomes more difficult for the metal atoms to diffuse through an increasing thickness of metal carbide interlayer such that there is no subsequent formation of metal carbide after the formation of a critical thickness of carbide interlayer. After a critical surface carbon concentration is reached, diamond can begin to nucleate if there are enough high energy sites (unsatisfied valences) on the surface. When graphite is formed as an interlayer, and there are enough high energy sites available on the surface, diamond will start to nucleate and grow preferentially compared to graphite due to the enhanced etching of graphite by hydrogen.

5. Summary

The intermediate layer formation at the interface between diamond and non-diamond substrates during diamond CVD is analyzed using thermodynamic QE model. Substrates of Si, Mo, W, Ti, Ta, Fe, and Ni are examined and the plausible intermediate layer formation on each is predicted as a function of deposition parameters. The advantages of the QE approach is that it minimizes the use of kinetics to the degree that the rate expressions are obtained without requiring the knowledge of the detailed kinetic models of the processes. The QE model predicts the formation of SiC, Mo_2C, TiC, TaC, WC, graphite and Fe_3C interlayers on Si, Mo, Ti, Ta, W, Ni, and Fe substrates for typical diamond CVD conditions. The model also predicts that, for growth of diamond, graphite, and carbides, the required CH_4/H_2 inlet ratio varies directly with reactor pressure, and inversely with substrate temperature. The predictions are in qualitative agreement with experimental and theoretical results available in the literature. In order for the QE model to make accurate quantitative predictions of the growth or etch rates, realistic values for the sticking coefficients of the reactants and for the desorption coefficients of the products from the substrate surface will be required. It has been postulated in the past that the excess carbon on the surface of a carbide interlayer is responsible for the nucleation of diamond. Consequently, future work will concentrate on calculating the critical thickness of a carbide interlayer, and the time required for a carbide layer to grow to a critical thickness, beyond which excess or 'free' carbon starts accumulating at the surface.

Acknowledgements

This work has been supported by the Materials Science Program at DARPA, Contract N00014-93-1-2002, and through partial support by Texas Instruments.

References

[1] K.E. Spear, J.P. Dismukes, Synthetic Diamond: Emerging CVD Science and Technology, Wiley, NY, USA, 1994.
[2] J.C. Angus, A. Argoitia, R. Gat, Z. Li, M. Sunkara, L. Wang, Y. Wang, Philos. Trans. Royal Soc., Ser. A 342 (1664) (1993) 195.
[3] S.D. Wolter, J.T. Glass, B.R. Stoner, J. Appl. Phys. 77 (10) (1995) 5119.
[4] S.D. Wolter, B.R. Stoner, J.T. Glass, P.J. Ellis, D.S. Buhaenko, C.E. Jenkins, P. Southworth, Appl. Phys. Lett. 62 (11) (1993) 1215.
[5] D. Kim, H. Lee, J. Lee, J. Mater. Sci. 28 (24) (1993) 6704.
[6] P.N. Barnes, R.L.C. Wu, Appl. Phys. Lett. 62 (1) (1993) 37.
[7] B.R. Stoner, S.R. Sahaida, J.P. Bade, P. Southworth, P.J. Ellis, J. Mater. Res. 8 (6) (1993) 1334.
[8] S.D. Wolter, B.R. Stoner, G.H.M. Ma, J.T. Glass, in: C.L. Renschler, J.J. Pouch, D.M. Cox (Eds.), Novel Forms of Carbon Symposium, Pittsburgh, PA, MRS (1992) p. 347.
[9] R. Csencsits, J. Rankin, R.E. Boekenhauer, M.K. Kundmann, B.W. Sheldon, in: H.A. Atwater, E. Chason, M.H. Grabow, M.G. Lagally (Eds.), Evolution of Surface and Thin Film Microstructure Symposium, Pittsburgh, PA, MRS, (1993) p. 695.
[10] T.P. Ong, F. Xiong, R.P.H. Chang, C.W. White, J. Mater. Res. 7 (9) (1992) 2429.
[11] M.M. Waite, S.I. Shah, Appl. Phys. Lett. 60 (19) (1992) 2344.
[12] A.A. Smolin, S.M. Pimenov, V.G. Ralchenko, T.V. Kononenko, V.I. Konov, E.N. Loubnin, Diamond Films Techn. 3 (1) (1993) 1.
[13] K. Tamaki, Y. Watanabe, Y. Nakamura, S. Hirayama, Thin Solid Films 236 (1–2) (1993) 115.
[14] X. Peng, H. Li, Mater. Lett. 17 (5) (1993) 223.
[15] G.A. Hirata, L. Cota-Araiza, M. Avalos-Borja, M.H. Farias, O. Contreras, Y. Matsumoto, J. Phys. 5 (33A) (1993) A305.
[16] J. Singh, J. Mater. Sci. 29 (10) (1994) 2761.
[17] J. Singh, M. Vellaikal, Surf. Coat. Technol. 64 (1994) 131.
[18] D.N. Belton, S.J. Schmieg, Thin Solid Films 212 (1–2) (1992) 68.
[19] W.R.L. Lambrecht, C.H. Lee, B. Segall, J.C. Angus, Z. Li, M. Sunkara, Nature 364 (6438) (1993) 607.
[20] B. Lux, R. Haubner, Diamond and Diamond-Like Films and Coatings, Plenum, New York (1991) p. 579.

[21] P.O. Joffreau, R. Haubner, B. Lux, Int. J. Ref. Hard Mater. 7 (4) (1988) 186.
[22] A. Lindlbauer, Ph.D Thesis, TU-Vienna, Austria (1991).
[23] D. Michau, B. Tanguy, G. Demazeau, M. Couzi, R. Cavagnat, Diamond Relat. Mater. 2 (1) (1993) 19.
[24] B.R. Stoner, G.H.M. Ma, S.D. Wolter, J.T. Glass, Phys. Rev. B 45 (19) (1992) 11067.
[25] K.V. Ravi, C.A. Koch, Appl. Phys. Lett. 57 (4) (1990) 348.
[26] R. Meilunas, M.S. Wong, K.C. Sheng, R.P.H. Chang, R.P. Van-Duyne, Appl. Phys. Lett. 54 (22) (1989) 2204.
[27] H. Liu, D.S. Dandy, Diamond Chemical Vapor Deposition: Nucleation and Early Growth Stages, Noyes Publications, NJ, 1995.
[28] J.C. Batty, R.E. Stickney, J. Chem. Phys. 51 (1969) 4475.
[29] M. Sommer, K. Mui, F.W. Smith, Solid State Commun. 69 (7) (1989) 775.
[30] R.-B. Wang, M. Sommer, F.W. Smith, J. Cryst. Growth 119 (1992) 271.
[31] E.H. Kennard, Kinetic Theory of Gases, McGraw-Hill, NY, 1938, p. 63.
[32] G.N. Lewis, M. Randall, Thermodynamics, McGraw-Hill, New York, 1961.
[33] J.C. Batty, Sc.D Thesis, MIT, (1969).
[34] I. Barin, Thermochemical Data of Pure Substances, VCH, NY, 1993.
[35] P. Mahalingam, Ph.D Thesis, Colorado State University, (1997).
[36] S. Matsumoto, Y. Sato, M. Tsutsumi, N. Setaka, J. Mater. Sci. 17 (1982) 3106.
[37] M. Katoh, H. Kawarada, Jpn. J. Appl. Phys. 34 (1995) 3628.
[38] M.L. Terranova, M. Rossi, G. Vitali, J. Appl. Phys. 80 (6) (1996) 3552.